Journal of Earth Sciences and Geotechnical Engineering, vol.6, no. 3, 2016, 17-34
ISSN: 1792-9040 (print version), 1792-9660 (online)
Scienpress Ltd, 2016

Theoretical GPR AVA Response of Rock Fractures: Implications for Aperture and Fill Characterization

Aisha Abubakar Kana[1]

Abstract

Rock fractures in the subsurface typically have apertures less than a wavelength of the dominant frequency of the GPR signal, thus generating complex reflectivity pattern. The resulting reflectivity is however useful as it depends on the fracture aperture and dielectric permittivity of the filling material. AVA analysis relates amplitude variations with increasing incidence angles and seeks to characterize interfaces and layers. In this paper, I present theoretical analysis of the AVA behaviour of thin fractures, assessing the sensitivity to fracture aperture and fill characteristics. The magnitude and curvature of the AVA curves depend on the fracture aperture and fill permittivity suggesting that fracture aperture and fill permittivity can be obtained from field measurements. Amplitude data for AVA analysis is collected in the field through CMP surveys. Converting these amplitude data for AVA analysis requires some careful but simplifying assumptions on the system under investigation, applying some amplitude corrections and offsets need to be converted to incidence angles. Fracture aperture and fill permittivity can then be constrained by fitting theoretical AVA curves for various fracture models to a field derived AVA curve.

Keywords: GPR, AVA, CMP, thin – layer, rock fractures

1 Introduction

Rock fractures typically have apertures less than a wavelength (λ) at the

[1] Department of Geology and Mining, Nasarawa State University, Keffi, Nigeria

dominant frequency of the GPR signal and as such generate complex reflectivity patterns due to interference from multiple reflections from their surfaces. Therefore, characterization of such fractures requires thin layer analysis [4]. AVA analysis is a multi – offset [12] attribute analysis technique which involves relating amplitude variations with increasing angle of incidence (or practically, offsets), in order to characterize interfaces and layers ([8]; [3]). Attribute analysis is a group of tools employed to quantify variations in the properties of a reflected waveform including its amplitude, frequency content and phase with incidence angle; and to relate these variations to the physical properties of the medium in which the signal is propagating and the reflecting interface or thin layer [5]. In seismic methods, attribute analysis is often used to associate shear and compressional wave properties with the presence of oil and natural gas ([8]; [6]). Attribute analysis of GPR data allows for exploitation of the information contained in a reflected wavelet, including geometry and detailed material property information.

The AVA technique has been successfully applied in seismic exploration to characterize contrasts in elastic properties at interfaces; it has proved a useful tool in hydrocarbon exploration ([15]; [8]). For media with electrical conductivity equal to or near 0 and magnetic permeability approaching 1, GPR (EM) waves behave qualitatively like seismic (shear) waves [12]. These assumptions are not always the case for earth materials but according to [9] they are reasonable approximations over the range of frequencies (10 – 1400 MHz) which a GPR signal will propagate efficiently in most materials. Applying the AVA technique to GPR data was first suggested by [2]; and later, [3] showed through analytical and numerical modelling that anomalous zones producing similar indistinguishable bi - static GPR responses (e.g. bright or dim spots in constant offset, CO, sections) can show very different behaviour when examined by AVA analysis. [7] Studied synthetic AVA curves for various contrasts in EM properties; they highlighted the potential of AVA analysis for characterizing non – aqueous phase liquid (NAPL) contamination, considering a single interface between an uncontaminated upper layer and a lower layer contaminated with NAPL. [10] Successfully characterized the presence of an NAPL contaminated zone at an alluvium/clay boundary using the AVA technique. These applications of the AVA method consider single interfaces separating media of contrasting electrical properties. [4] Investigated the AVA response of a thin layer using an analytic solution to the reflectivity from the top of the thin layer and successfully identified a thin NAPL contaminated layer in the saturated zone. Successful application of thin layer AVA analysis in characterizing hydrocarbon contamination in the subsurface suggests the method can be extended to subsurface fracture characterization as both targets are qualitatively similar i.e. thin layers [4]. In line with the thin layer approach outlined in [4], [11] studied dispersive i.e. frequency dependent amplitude and phase variation with offset (APVO) curves for a restricted case of a thin layer embedded within a homogeneous rock, and assessed

its potential for characterizing the aperture and fill of such layers. Their approach to estimating thin layer aperture and fill is an inversion scheme which compares, in the frequency domain, field data with synthetic data generated from analytical solutions to thin layer reflection coefficients. They applied the methodology to CMP data acquired over a vertical fracture on a cliff face and successfully characterized the aperture (0.4m) and fill relative permittivity (3.1). The AVA technique has previously not been applied to thin fractures such as typically encountered in the subsurface. In this paper, I present theoretical analyses of thin ($\leq 0.5\ \lambda$) fracture AVA for two cases: (1) a fracture embedded in a homogeneous rock; and (2) a fracture embedded in a homogeneous half space of different relative permittivity. I begin with an overview of the AVA method; I then illustrate with some examples, fracture AVA sensitivity to aperture and fill permittivity; finally, I discuss some practical considerations in acquiring data for AVA analysis from field surveys.

2 The AVA method

Conventional GPR data are collected with a constant antenna separation or offset (CO), but for AVA analysis, GPR data must be collected using the common mid - point (CMP) survey geometry. In the CMP mode, antennas are moved symmetrically about a midpoint increasing the offset, and data collected for the same point on a reflector (assuming a horizontal interface) so that the reflections are recorded for each antenna offset.

Table 1. Factors affecting a reflected GPR signal, modified from [5].

Factor	**Remarks**
Reflection coefficients versus incidence angle (offset)	Signal, which is sought after in AVA analysis
Composite reflection from multiple interfaces	Potential information (considered noise or signal depending on the analysis)
Tuning as a result of NMO convergence Antennae coupling; random noise; instrumentation	Noise - *offset dependent*
Source/receiver directivity; emergence angles; coherent noise/multiples; **spherical spreading**; processing distortions, NMO errors and stretch; intrinsic **attenuation** and anisotropy; transmission coefficients and scattering above target of interest; structural complexity	Noise - *offset dependent*

The antenna offset is subsequently converted to angle of incidence; a plot of reflection amplitudes against the angle of incidence represents the main diagnostic data for AVA analysis ([8]; [3]). The recorded amplitude (A_{obs} (mV)) can be expressed as:

$$\boldsymbol{A_{obs} = A_{sou} . \frac{C_{TR} . P_{TR} . t}{r} . R . exp^{(-\alpha r)}} \quad (1)$$

Where: C_{TR} is antennae coupling with the ground surface; *t* here is defined as transmission loss through any interface in the overburden above the target reflection; P_{TR} is antennae pattern; A_{sou} *(mV)* is the source amplitude; α *(m^{-1})* is the attenuation coefficient; r (m) is the ray path length. *R* is the absolute reflection coefficient.

In table 1, reflection coefficients versus incidence angle are of interest in AVA analysis. Other factors like geometric spreading (*S*); intrinsic attenuation in the propagating medium ($exp^{(-\alpha r)}$); transmission losses across interfaces above the target reflection (*t*); and antennae (transmitter and receiver) patterns (P_{TR}) are important sources of noise which must be accounted for in AVA analysis.

It therefore becomes necessary to make some careful but justified assumptions on the system under investigation which are: frequency independent electrical properties [1]; constant antennae coupling with the ground surface, and constant transmission losses due to any reflections above the target reflection, for range of offsets considered [5]. To justify the latter assumptions, the surface over which measurements are made must be uniform (i.e. smooth) with a homogeneous surface material, and strata in the overburden must be planer, horizontal and parallel to the ground surface. [4] Conclude that errors associated with assuming constant transmission losses are less than 5% for incidence angles up to 65% of the critical angle for increasing velocity with depth. For decreasing velocity with depth, the assumption is valid for incidence angles from 35° to 55°. Information on the absolute source amplitude in GPR is difficult to obtain, it is therefore necessary to normalize the observed amplitudes e.g. by a near offset amplitude or the maximum amplitude. The reflection amplitude ratio can be written as:

$$\boldsymbol{\frac{A_{obs\,(\theta)}}{A_{obs(\theta=90)}} = \frac{R_\theta . P_{TR\theta} . r_{\theta=90}}{R_{\theta=0} . P_{TR(\theta=90)} . r_\theta} . exp^{-\alpha(r_\theta - r_{\theta=90})}} \quad (2)$$

By correcting for antennae pattern, geometric spreading and intrinsic attenuation, the normalized amplitude at a given angle of incidence approximates the

normalized reflection coefficient *R* i.e.:

$$\frac{A_{corr\,\theta}}{A_{corr\theta=90}} = \frac{R_{\theta}}{R_{\theta=90}} \tag{3}$$

The resulting normalized reflection amplitudes can then be compared with normalized theoretical amplitudes (1) in order to constrain interface and layer properties.

The choice of amplitude for quantitative AVA analysis is also crucial. Although frequency independence is assumed, artefacts associated with phase rotation are still observed in GPR wavelets, as illustrated in [5], who suggested using the maximum of the envelope function (or Hilbert transform, see [16]) calculated over the duration of a wavelet, which is more appropriate and devoid of phase related artefacts.

For the following analysis, I consider only transverse electric, *TE* mode data, and unless otherwise stated, amplitude is defined as the local maximum of the envelope function or Hilbert transform [16]' calculated over the duration of the signal.

3 Fracture aperture and fill characterization from AVA analysis

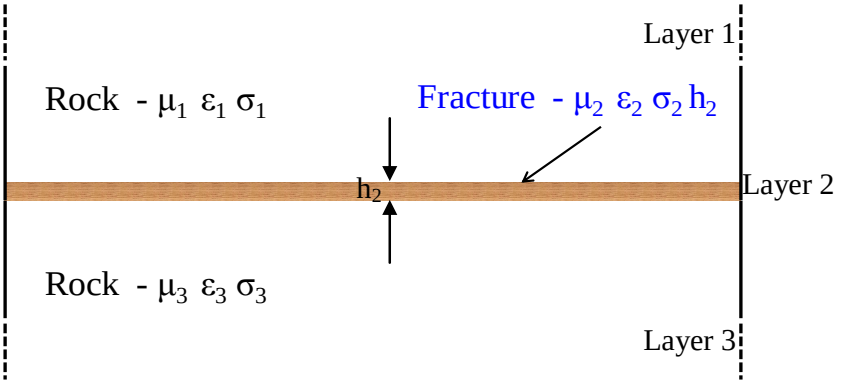

Figure 1. Rock fracture model.

Considering the thin fracture in figure 1, an analytic solution to the *TE* mode reflectivity from the surface of the fracture is given by equation 4, modified from [14] by [4]. The equation quantifies the amplitude reflection coefficient, *R*, for a system comprising the rock (layers 1 & 3), separated by the fracture (layer 2) of a finite thickness (h_2).

$$\mathbf{R_{TE}} = \frac{\boldsymbol{\gamma_1} - \boldsymbol{\gamma_3} - \mathbf{i}\left(\frac{\boldsymbol{\gamma_1\gamma_3}}{\boldsymbol{\gamma_2}} - \boldsymbol{\gamma_2}\right)\tan(\boldsymbol{\gamma_2 h_2})}{\boldsymbol{\gamma_1} + \boldsymbol{\gamma_3} - \mathbf{i}\left(\frac{\boldsymbol{\gamma_1\gamma_3}}{\boldsymbol{\gamma_2}} + \boldsymbol{\gamma_2}\right)\tan(\boldsymbol{\gamma_2 h_2})} \tag{4}$$

$$\gamma_n = \omega\sqrt{\varepsilon_n \mu}\, cos\, \theta_n \tag{5}$$

$$\cos\theta_n = \left[1 - \frac{\varepsilon_1 \sin^2\theta_1}{\varepsilon_n}\right]^{1/2} \tag{6}$$

$$\omega = 2\pi f$$

Where ε is dielectric permittivity (F/m), θ is angle of incidence (deg) in at the base of the *nth* layer, ω is angular frequency (Hz), μ is vacuum magnetic permeability (H/m), h_2 is thickness of the thin fracture (m), i is $\sqrt{-1}$, and γ is wave number. Subscripts 1, 2, 3 & *n* refer to layers 1, 2, 3 & *n* respectively.

4 Theoretical AVA curves for various fracture models

For a 'clean' (i.e. no alteration along surfaces) fracture with smooth, parallel and planar surfaces; uniform plane waves propagating in a non – conductive (σ = 0), homogeneous and isotropic rock with frequency independent properties and magnetic permeability equal to that of free space (μ_r = 1), equation 1 shows that fracture reflectivity depends on: the dielectric permittivity of the host rock and the fracture itself; fracture aperture; angle of incidence; and polarization of the incident EM wave.

To illustrate the sensitivity of fracture AVA to aperture and fill characteristics, I computed the reflected amplitudes for a broadband signal with a centre frequency of 500 MHz, evaluated at increasing angle of incidence, hence normalized AVA curves, for various fracture aperture and fill permittivity values. The computations were done using the broadband model described in [4] for computing TE mode reflection coefficients from the top of a three layer sequence. In the model, a source spectrum is filtered with equation 1, and the inverse Fourier transform of the filtered spectrum gives the time domain response or the reflected wavelet. The maximum of the envelope function for the reflected wavelet is then

taken. In [4] a Ricker wavelet was used as the source wavelet; here, I use a wavelet which I recorded with 500 MHz Sensors and Software antennae put together i.e. facing each other (figure 2).

The procedure was coded in MATLAB® and AVA curves were computed for air ($\varepsilon_{r2} = 1$), dry clay ($\varepsilon_{r2} = 2$), wet sand ($\varepsilon_{r2} = 40$) and water ($\varepsilon_{r2} = 80$) filled fractures in limestone of $\varepsilon_{r1} = 10$ above and below the fracture. The computation was repeated for the case where rock above and below the fracture have different relative permittivity (i.e. $\varepsilon_{r1} = 10 > \varepsilon_{r3} = 7$). The parameter space (i.e. aperture, h_2 and fill permittivity, ε_{r2}) and corresponding $h2{:}\lambda$ ratio is shown in figure 3. The permittivity range for most geological materials is between 2 and 40, the limits being equivalent to dry clay and wet clay respectively (red box in figure 3). Thin layer analysis is necessary when h_2 is less than 0.75λ (black curve in figure 4).

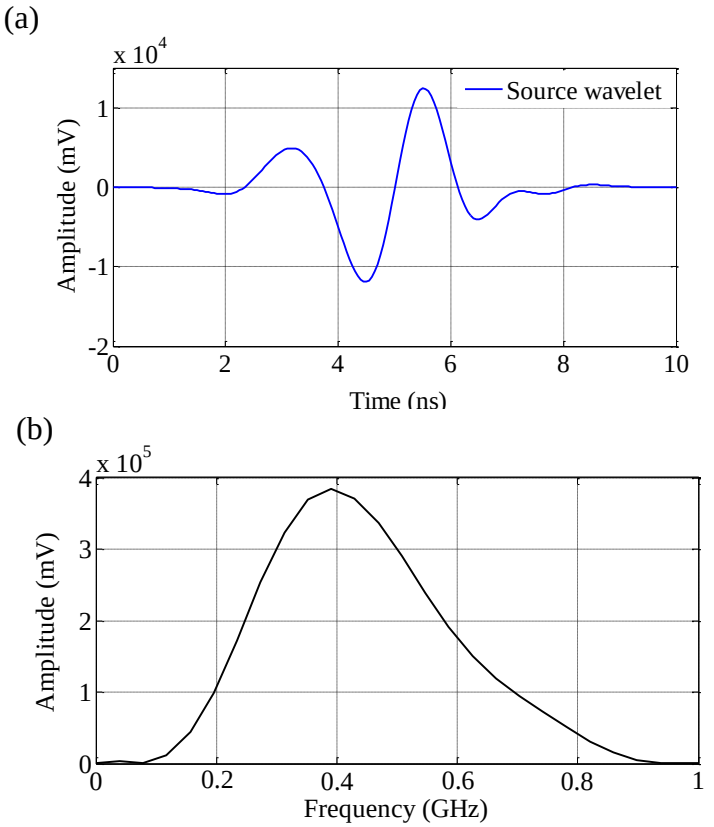

Figure 2. Source wavelet (a) and corresponding source spectrum (b) used to compute the reflected field from the top of a thin fracture.

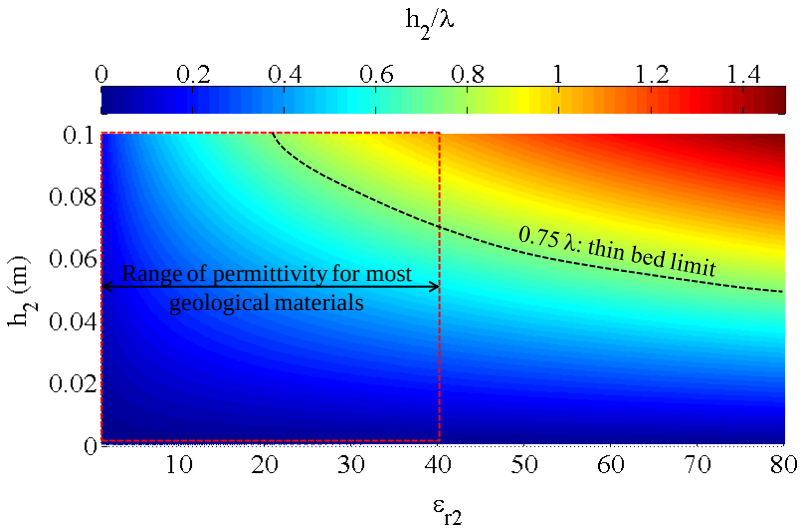

Figure 3. Parameter (h_2, ε_{r2}) space and corresponding thickness – wavelength ratio.

The AVA curves in figures 4 to 7 show that the amplitude *R*, generally increases from a minimum at normal incidence ($\theta_i = 0°$) up to a maximum at $\theta_i = 90°$. *R* curve is initially flat (at low θ_i) and only becomes sensitive to θ_i at $\theta_i > 20°$ for fractures filled with wet sand and water (figures 6 and 7). *R* magnitude and the shape or curvature of the AVA curve depends on fracture aperture (especially in air and dry clay filled fractures, figures 4 and 5), fill permittivity and on permittivity contrasts in the host rock above and below the fracture. Except for dry clay and air filled fractures (figures 4 and 5), *R* magnitude is highest at an aperture equivalent to 0.25λ in each case (dashed line).

(a)

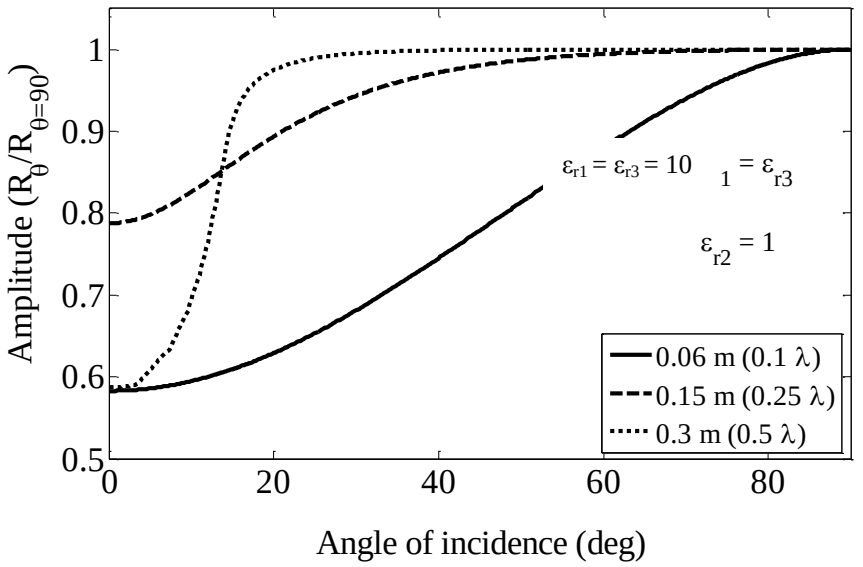

(b)

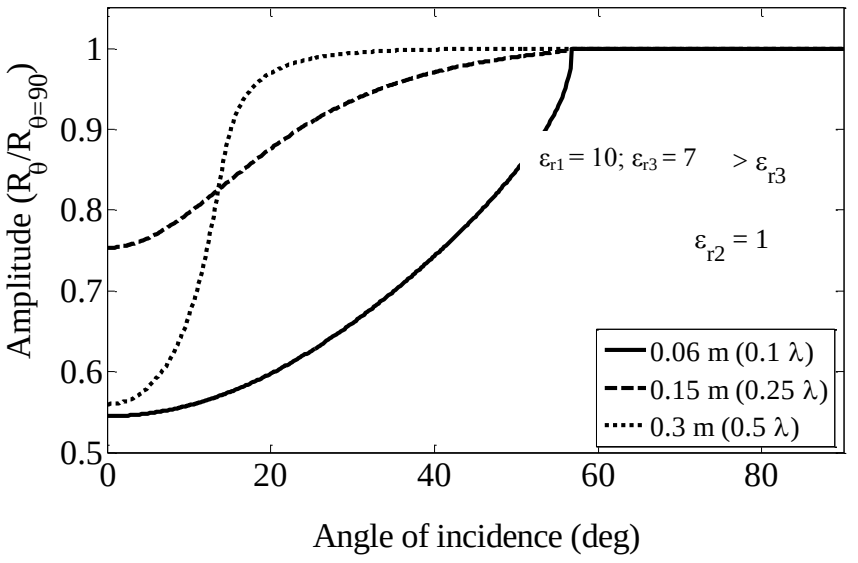

Figure 4 Theoretical AVA curves for a water filled fracture where (a) $\varepsilon_{r1} = \varepsilon_{r3}$ and (b) $\varepsilon_{r1} > \varepsilon_{r3}$. The different curves correspond to different fracture thicknesses, expressed in wavelengths at the dominant frequency.

(a)

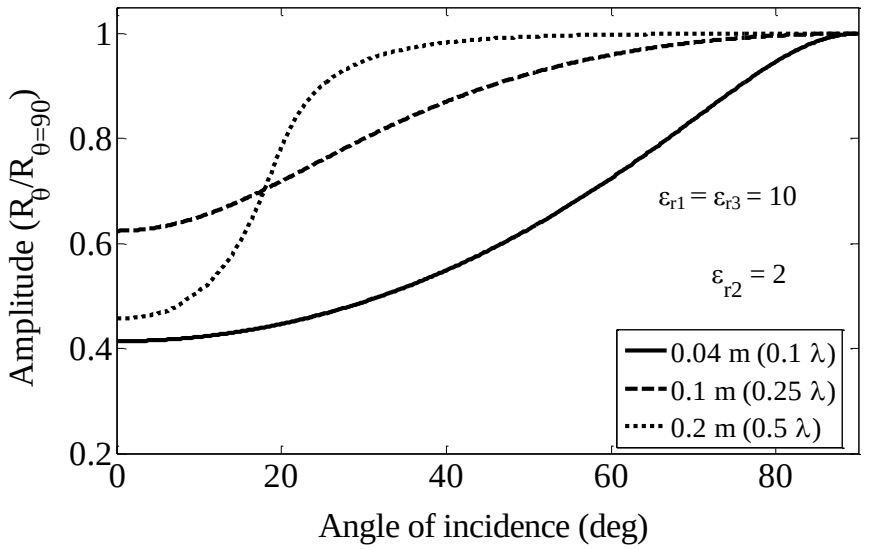

(b)

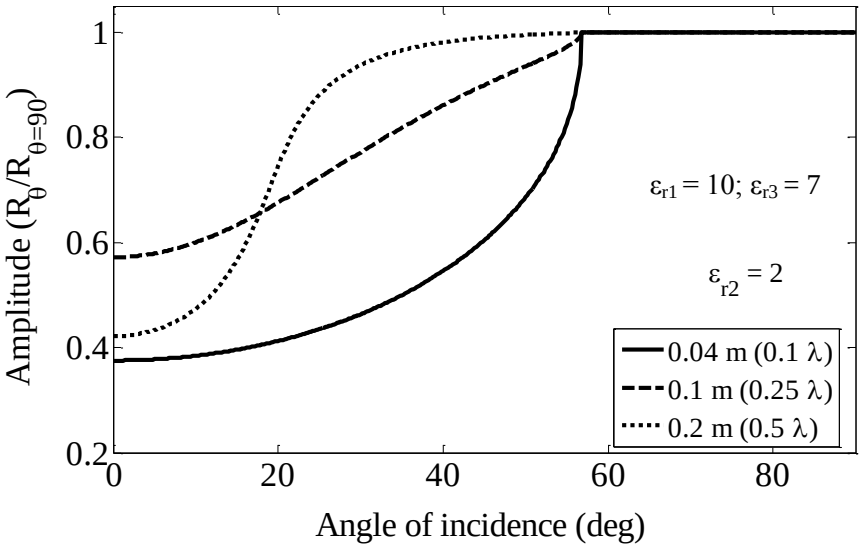

Figure 5. Theoretical AVA curves for a dry clay filled fracture where (a) $\varepsilon_{r1} = \varepsilon_{r3}$ and (b) $\varepsilon_{r1} > \varepsilon_{r3}$. The different curves correspond to different fracture thicknesses, expressed in wavelengths at the dominant frequency.

(a)

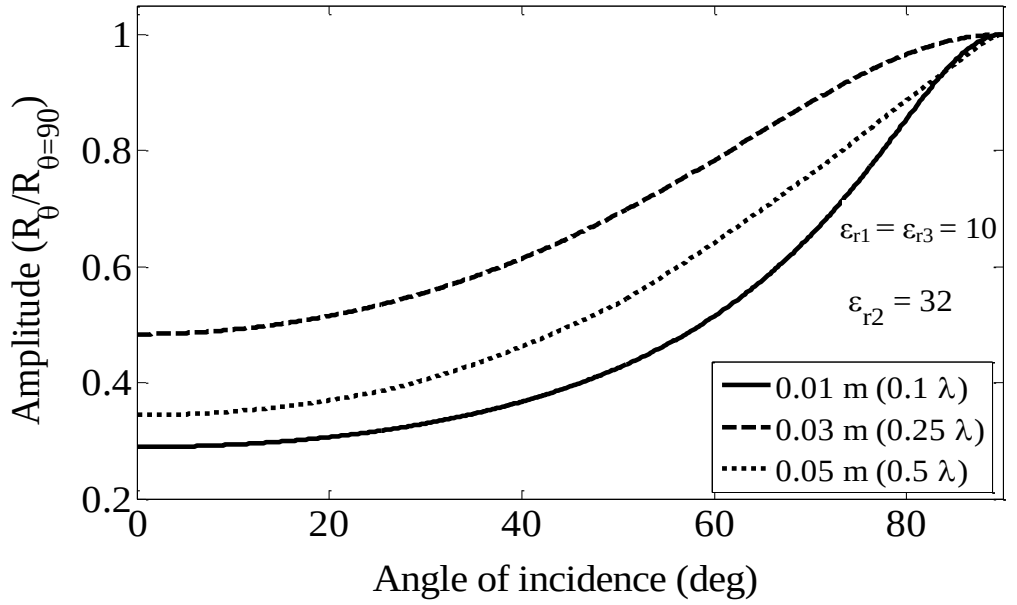

(b)

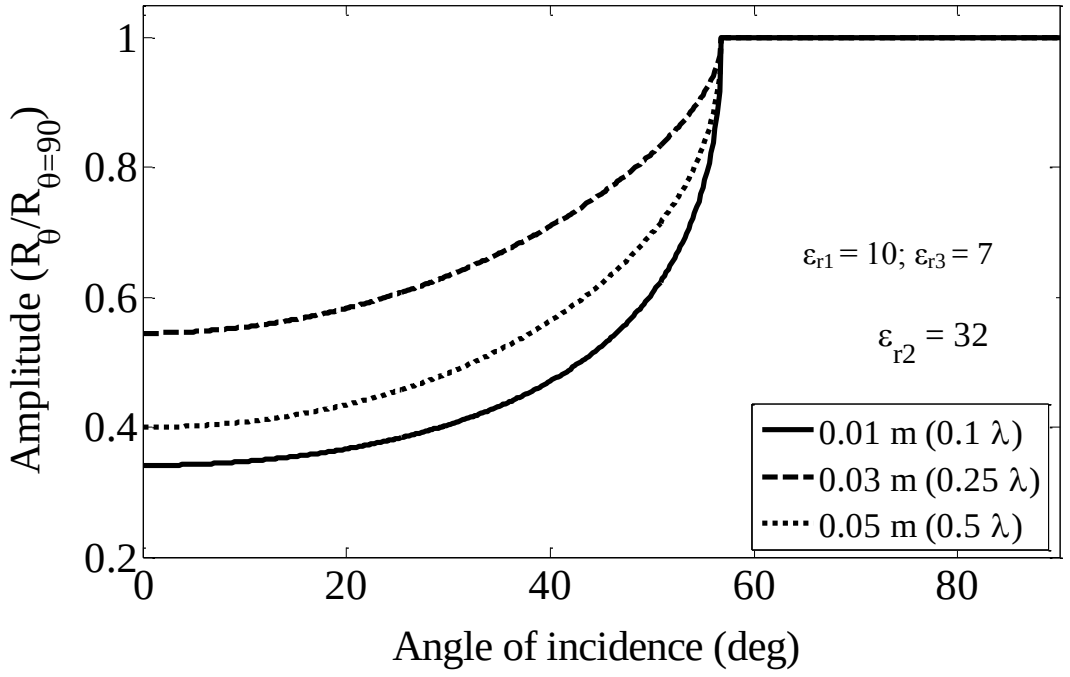

Figure 6. Theoretical AVA curves for a wet sand filled fracture where (a) $\varepsilon_{r1} = \varepsilon_{r3}$ and (b) $\varepsilon_{r1} > \varepsilon_{r3}$. The different curves correspond to different fracture thicknesses, expressed in wavelengths at the dominant frequency.

(a)

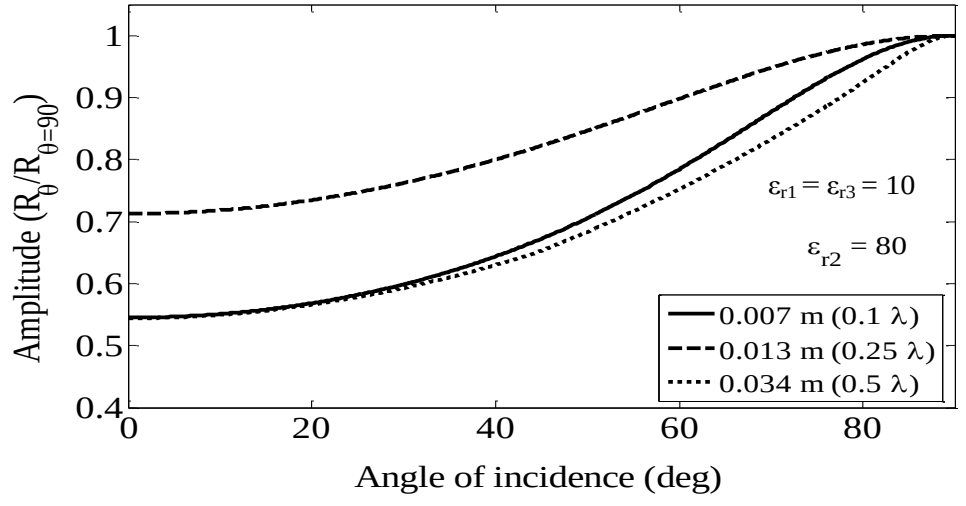

(b)

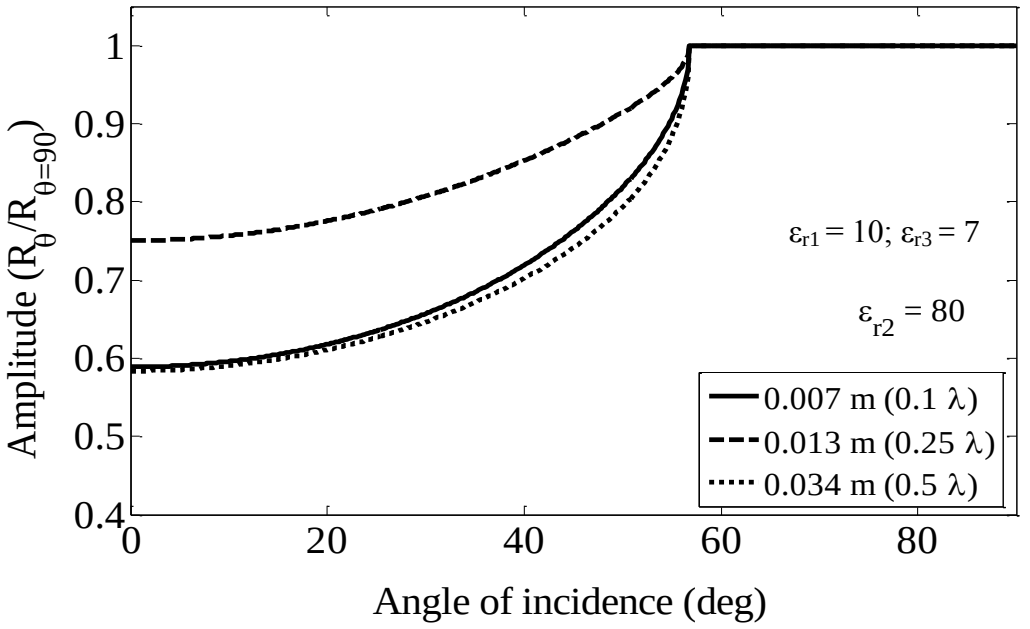

Figure 7. Theoretical AVA curves for a water filled fracture where (a) $\varepsilon_{r1} = \varepsilon_{r3}$ and (b) $\varepsilon_{r1} > \varepsilon_{r3}$. The different curves correspond to different fracture thicknesses, expressed in wavelengths at the dominant frequency.

In the case where the host rock is not homogeneous i.e. rock above and below the fracture have different electrical properties ((b) in each case), the reflectivity is a composite of two reflections: one which will result if there was no fracture (i.e. due to ε_{r1} - ε_{r3} contrast) and an interference product of reflections from the surfaces defining the fracture i.e. due to ε_{r1} - ε_{r2} and ε_{r2} - ε_{r3} contrast (Widess, 1973). The influence of the layer 1 - layer 3 contrast is seen in figures 4 b to 7b where total internal reflection beyond the critical angle of incidence (in this case ~ 58°) evidenced by flattening of the AVA curves is observed.

In the air and dry clay filled fractures embedded in a homogeneous rock (figures 4a and 5a), total internal reflection beyond the critical angle between layer 1 and the fracture (18°) is only seen in the 0.5λ thick fracture. Although the entire incident wave is reflected back into layer 1, there is some penetration, travelling as an evanescent wave along the layer 1 - fracture boundary. This wave exists to obey EM boundary conditions (continuity of the electric and magnetic flux densities orthogonal to the interface, and continuity of the tangential electric and magnetic fields across the interface), but decays rapidly with distance, in the

absence of a third medium within 0.3λ of the boundary; as such, the wave does not transmit energy into the fracture and total internal reflection is observed (figure 8a). In the presence of a third medium close to the boundary, which is the case for the fracture here, the evanescent wave will not decay much before it reaches the boundary between the fracture and layer 3, where it is partially reflected back into the fracture and partially transmitted into layer 3 (figure 8b). This explains why total internal reflection is not observed in the 0.1λ and 0.25λ thick fractures.

(a)

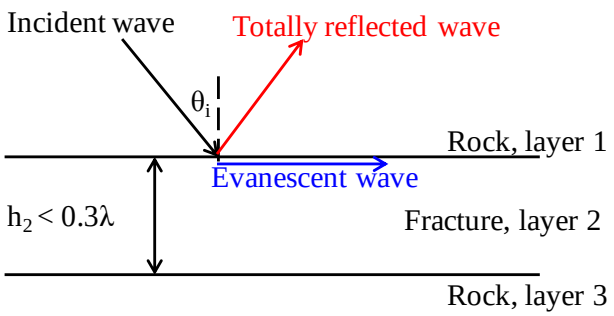

(b)

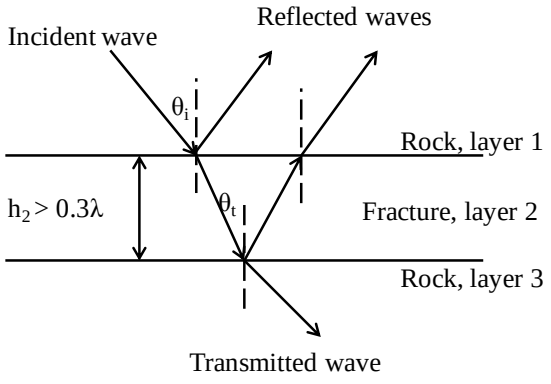

Figure 8. Evanescent waves in (a) a fracture with $h_2 < 0.3\lambda$ and (b) $h_2 > 0.3\lambda$. See text for explanation.

The preceding explanation applies to the inhomogeneous host rock case; however, the total internal reflection observed in fractures narrower than 0.3λ is due to the dielectric contrast between the host rock above and below the fracture i.e. $\varepsilon_{r1} > \varepsilon_{r3}$.

The characteristics of the AVA curve especially its dependence on aperture and fill material suggests its potential for characterising fractures if the fracture AVA can be measured from field surveys. However, the contrast in electrical properties

between the fracture and the host rock must be significant in order to detect the fracture and observe the AVA characteristics outlined above.

6 Practical considerations

A practical approach to fracture characterization using the AVA method involves extracting AVA characteristics from field CMP data. Practical considerations mainly concern the design of CMP surveys, including identifying suitable reflections and achieving sufficiently long offsets or wide incidence angles, in order to observe the AVA characteristics. [4] suggest collecting a CO profile first, and from the profile, identifying relatively distinct reflections for subsequent CMP surveys; hence, the choice of CO offset (antennae separation) is crucial. Identifying reflections depends on the degree of contrast in dielectric properties from the host rock.

Theoretical AVA curves in figures 4 to 7 show that wide incidence angles are required to observe the AVA characteristics especially in fractures that contain water or a wet filling material. Achieving wide incidence angles (offsets) depends on target reflector depth, and the character of any velocity variation in the overburden (above the target reflection). Shallow reflections allow access to wide incidence angles but with these, it will be difficult to access amplitude data at wider offsets (angles) due to interference from the direct ground wave.

The velocity structure in a CMP section also affects the range of incidence angles for a particular reflection. Most subsurface models are characterized by decreasing interval velocity with depth because of increasing moisture content with depth as the water table is reached. This structure results in ray bending towards the normal, decreasing the incidence angle with depth. This will limit the maximum incidence angle in lower layers (e.g. f_1 in figure 9) because of total internal reflection beyond the critical angle. In designing a CMP survey, prior information on the nature of the rock under investigation is required especially on velocity.

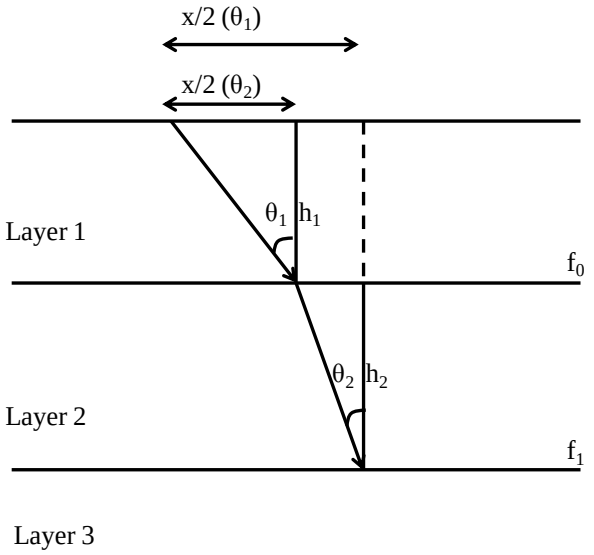

Figure 9. A simple ray path through layers 1, 2 and 3, showing the reflections: f_0 at layer1 – layer 2 boundary and f_1 at layer 2 – layer 3 boundary.

With prior knowledge on the velocity, the offset required to achieve a particular angle of incidence for f_0 in figure 9 can be calculated from equation 7, while the offset for f_1 is given by equation 8 from [4].

$$\frac{X}{2}(\theta_1) = \tan\theta_1 \,.h_1 \tag{7}$$

$$\frac{X}{2}(\theta_2) = h_1 \,.\tan\left[sin^{-1}\left(\sqrt{\frac{\varepsilon_2}{\varepsilon_1}}\,\sin\theta_2\right)\right] + h_2 \,.\tan\theta_2 \tag{8}$$

Where: h is layer thickness, ε is permittivity, and X is offset. Subscripts 1 and 2 correspond to layers 1 and 2 respectively.

Figures 10a to 10c are predicted offsets required to achieve 20° and 45° incidence angles at f_0 and f_1 (figure 9) computed using equations 7 and 8. In all figures, offsets required to achieve the investigated incidence angles increase with depths to reflectors. In the case where: $\varepsilon_{r1} > \varepsilon_{r3}$, relatively (relative to the case where: $\varepsilon_{r1} < \varepsilon_{r3}$) wider offsets (at a particular depth to reflector) are required to achieve the investigated incidence angles, due to ray bending towards the normal, as offsets are increased.

(a)

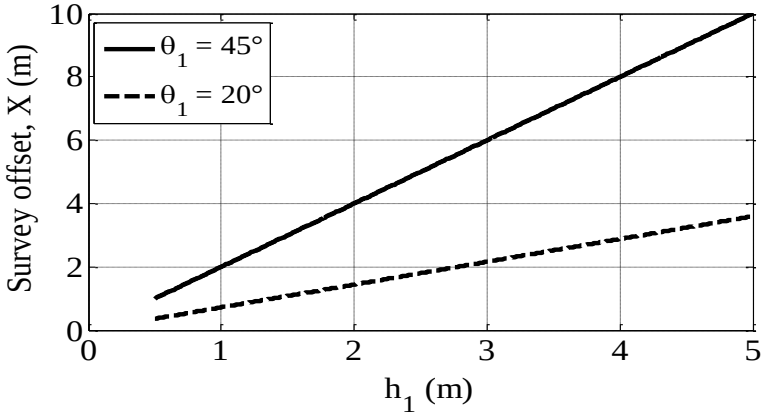

(b)

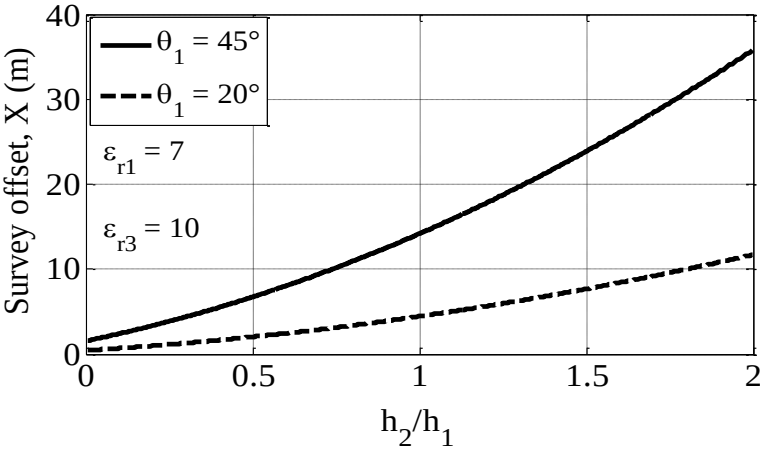

(c)

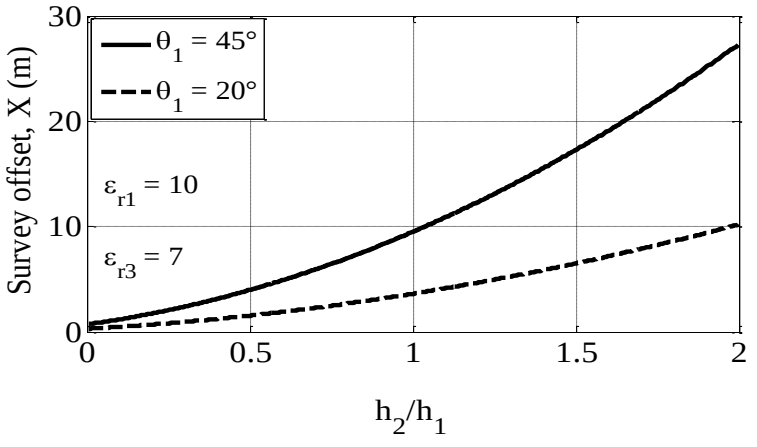

Figure 10. Range of survey offsets, required to achieve 20° and 45° incidence at (a) f_0, (b) f_1 for $\varepsilon_{r1} < \varepsilon_{r3}$; and (c) f_1 for $\varepsilon_{r1} > \varepsilon_{r3}$, for increasing depth to reflector.

7 Conclusion

In this paper, I presented the theoretical basis for fracture characterization using the GPR thin layer AVA method and how fracture amplitude data can be collected from the field and analysed with the method. I illustrated the sensitivity of thin layer AVA characteristics on the thin layer thickness and dielectric permittivity of the filling material using synthetic AVA curves. I generated AVA curves for various fracture models using a broadband model. The magnitude and curvature of the AVA curves depend on the fracture aperture and fill permittivity suggesting that fracture aperture and fill permittivity can be obtained from field measurements. Amplitude data for AVA analysis is collected in the field through CMP surveys. Converting these amplitude data for AVA analysis requires some careful but simplifying assumptions on the system under investigation, applying some amplitude corrections and offsets need to be converted to incidence angles. Fracture aperture and fill permittivity can then be constrained by fitting theoretical AVA curves for various fracture models to a field derived AVA curve.

References

[1] Annan A. P. Transmission Dispersion and GPR. *Journal of Environmental and Engineering Geophysics*, **0**, (1996), pp 125-136.

[2] Baker G. S., Clement W. P., and Smith S. B. Amplitude and phase variations with offset in ground penetrating radar for identifying dense and light non-aqueous phase liquid contaminants, paper presented at Geological Society of America National meeting, Nov 6th - 9th 1995.

[3] Baker G. S. Applying AVO analysis to GPR data. *Geophysical Research Letters*, **25**, (1998), pp 397- 400.

[4] Bradford J. H., and Deeds J. D. Ground-penetrating radar theory and application of thin-bed offset dependent reflectivity. *Geophysics* **71**, (2006), pp K147 - K157.

[5] Bradford J. H. Characterizing shallow aquifers with wave- propagation based geophysical techniques: Imaging and attribute analysis. *PhD Thesis.* Rice (1998).

[6] Bradford J.H., and Wu Y. Time-frequency representation of seismic signals via matching pursuit decomposition with complex Ricker wavelets. *AGU Fall meeting.* San Francisco: American Geophysical Union, (1997).

[7] Carcione J., M. Botelho A. Osella and M. de la Vegas. Fresnel reflection coefficients for GPR - AVO analysis and detection of sea water and NAPL contaminants. *Near Surface Geophysics*, **71**, (2006) pp 253–263.

[8] Castagna J. P. AVO analysis – Tutorial and review in: Castagna J. P and Backus M. M ed. Offset Dependent Reflectivity – Theory and Practice of AVO analysis. Society of Exploration Geophysicists, USA, (1993) pp 3 - 36.

[9] J. L., and Annan A. P. Ground - penetrating radar for high resolution mapping of soil and rock stratigraphy. *Geophysical prospecting,* **37,** (1989) pp 531 - 551.

[10] Deeds J. D., and Bradford J. H. Characterization of an aquitard and direct detection of LNAPL at Hill Air Force Base using GPR AVO and migration velocity analysis. *9th International Conference on Ground Penetrating Radar, International society for Optical Engineering Proceedings*, 5 -19, (2002).

[11] Deparis J., and Garambois S. On the use of dispersive APVO GPR curves for thin-bed properties estimation: Theory and application to fracture characterization. *Geophysics*, **74**, (2009) pp J1 - J12.

[12] Fisher E., McMechan G. A., and Annan A. P. Acquisition and processing of wide-aperture ground-penetrating radar data. *Geophysics*, **57**, (1992) pp 495 - 504.

[13] Inan S. U., and Inan S. A. Electromagnetic waves. Prentice – Hall, Inc, upper Saddle River, USA, (2000).

[14] King R. W. P., and Owens M. Lateral electromagnetic waves: Theory and applications to Communication, Geophysical prospecting and Remote sensing. Springer - Verlag, New York, (1992).

[15] Ostrander W. J. Plane-wave reflection coefficients for gas sands at non-normal angles of incidence. G*eophysics*, **49**, (1984) pp. 1637-1648.

[16] Sheriff, R. E. Encyclopedic dictionary of Geophysics. Society of Exploration Geophysicists SEG, (2000).